

Combining GAN and LSTM Models for 3D Reconstruction of Lung Tumors from CT Scans

Cong Gu^{1*}, Hongling Gao²

College of Science, Zhongyuan University of Technology, Zhengzhou 450007, Henan, China¹
University Hospital, Zhongyuan University of Technology, Zhengzhou 450007, Henan, China²

Abstract—Generating a three-dimensional (3D) reconstruction of tumors is an efficient technique for obtaining accurate and highly detailed visualization of the structures of tumors. To create a 3D tumor model, a collection of 2D imaging data is required, including images from CT imaging. Generative adversarial networks (GANs) offer a method to learn helpful representations without annotating the training dataset considerably. The article proposes a technique for creating a 3D model of lung tumors from CT scans using a combination of GAN and LSTM models, with support from ResNet as a feature extractor for the 2D images. The model presented in this article involves three steps, starting with the segmentation of the lung, then the segmentation of the tumor, and concluding with the creation of a 3D reconstruction of the lung tumor. The segmentation of the lung and tumor is conducted utilizing snake optimization and Gustafson–Kessel (GK) method. To prepare the 3D reconstruction component for training, the ResNet model that has been pre-trained is utilized to capture characteristics from 2D lung tumor images. Subsequently, the series of characteristics that have been extracted are fed into a LSTM network to generate compressed features as the final output. Ultimately, the condensed feature is utilized as input for the GAN framework, in which the generator is accountable for generating a sophisticated 3D lung tumor image. Simultaneously, the discriminator evaluates whether the 3D lung tumor image produced by the generator is authentic or synthetic. This model is the initial attempt that utilizes a GAN model as a means for reconstructing 3D lung tumors. The suggested model is evaluated against traditional approaches using the LUNA dataset and standard evaluation metrics. The empirical findings suggest that the suggested approach shows a sufficient level of performance in comparison to other methods that are vying for the same objective.

Keywords—3D tumor reconstruction; lung cancer; LSTM; Generative adversarial network; ResNet

I. INTRODUCTION

Among men, lung cancer is the cancer type that occurs the second most frequently. In recent times, a number of data-based tools have been created by researchers to assist in the diagnosis and treatment of this condition. The ability to comprehend the 2D/3D shape of a tumor is crucial for visualizing the progression of its growth and for surgical purposes. 3D images offer comprehensive insights into the form and structure of the tumor [1].

CT is the favored imaging method for the detection of lung tumors among a variety of diagnostic imaging methods. Despite the fact that CT provides valuable information about

tumors, evaluating an increasing number of images can pose a challenge for radiologists, potentially creating risks. Consequently, it is crucial to create intelligent diagnostic approaches that can aid radiologists and doctors in making faster and more accurate judgments than those reliant exclusively on CT images [2].

Recently, several studies have been conducted on 3D tumor healing with a special focus on healing brain tumors. Although these methods have achieved promising results, they fail to offer a high-quality 3D reconstruction of lung tumors. This is due to the fact that tumors may have complex and random shapes. Additionally, high-quality 3D reconstruction heavily relies on the availability of accurate data in all three dimensions. To the knowledge, the most recent study [3] utilizes conventional methods to reconstruct lung cancer in three dimensions. In this study, significant characteristics are identified from a two-dimensional shape during the reconstruction process. This method includes multiple stages, such as surface reconstruction and smoothing, which can be computationally intensive. As a result, applying this approach in real-world situations where time is a crucial factor may be impractical. Furthermore, the proposed approach is tailored exclusively to lung tumors and may not be readily adaptable to other types of tumors or organs. Convolutional neural networks (CNNs) are capable of automatic feature extraction. Nonetheless, teaching CNNs necessitates a substantial quantity of classified information, which may be lacking, particularly in the medical sector. The processing power and memory requirements for CNNs training may also be high. Transfer learning (TL) may be used instead of training from scratch to deal with these difficulties. In TL, CNNs parameters are set to the values that have been trained on large-scale datasets. Many TL networks, particularly ResNet, have achieved satisfactory results in medical imaging applications [4]. The use of GAN in medical image reconstruction is not extensively studied [5]. Wang et al. [6] developed an U-Net model with skip connections that are sparse by merging two GAN methods, an encoder-decoder method, and an U-Net method, to enhance imaging quality and decrease the size of imaging equipment. Meanwhile, Yang et al. [7] created a generator network with skip connections based on the U-Net architecture, and they also incorporated a refinement learning approach to ensure the stability of GAN training and facilitate faster convergence with less parameter tuning. Despite achieving satisfactory results in their respective tasks, these methods lack the ability to perform 3D reconstruction of lung tumors.

To produce a 3D image, it is vital to extract a comprehensive representation from a series of 2D images in the form of a single vector that encapsulates all the necessary details. Recursive networks, such as LSTM [8], can address this challenge and have been found to be suitable for sequence data in previous studies [9, 10]. LSTM utilizes special blocks called cells. Each cell has three gates: input, output, and forget [11]. The input gate handles the storage of new information in the cell. The output gate is responsible for selecting which portion of the cell state should be transmitted to the cell's output. The forget cell is responsible for forgetting (throwing away) data as time passes, which helps with the vanishing gradient problem [12].

A GAN is composed of two neural networks, namely a generator and a discriminator. The generator creates synthetic data, and the discriminator attempts to tell actual samples from synthetic ones. The GAN model's capacity to generate superior synthetic data has made it highly popular in academics and business. Promising outcomes have been demonstrated by using GAN in different fields of application, including but not limited to generating high-resolution images, translating text to images, and transforming images to other types of images [13]. Acceptable generalization can be achieved by training DNNs using a combination of limited real data and large amounts of synthetic data generated by GANs. The creative technique of GANs has been employed in diverse medical imaging assignments, such as image partitioning, image enhancement, and image creation. By instructing the generator network on an extensive compilation of images, GANs can produce fresh images that have corresponding attributes to the source dataset. In medical imaging, this has been used to create new images that can help diagnose diseases or assist in surgical planning. On the other hand, the discriminative approach of GANs has been used to improve the quality of medical images. Discriminative GANs aim to distinguish between real and fake images and use this information to improve the generator network. By doing so, discriminative GANs can learn to regularize or normalize images and remove any artifacts or noise that might be present. Both approaches have shown great promise in medical imaging, and researchers are continually exploring new ways to apply GANs in this field. However, challenges remain, such as the need for large datasets and the difficulty of interpreting the outputs of GANs. Nevertheless, the potential benefits of GANs in medical imaging make it an area of active research and development [14].

For this study, a GAN-driven approach is suggested to produce 3D lung tumor reconstructions. The procedure comprises of three steps: segmentation of the lung, segmentation of the tumor, and creation of a 3D representation. The first stage employs the snake optimization method [15] to identify the left and right lungs. The suggested method simplifies the complexity of the issue by dividing it into multiple lower-dimensional problems with search areas that are gradually reduced [16]. The second stage utilizes GK clustering [17] to segment tumors and extract tumor masses from the affected lungs. The third stage involves an LSTM and a GAN. Initially, a pre-trained ResNet model extracts features from 2D lung tumor images, and subsequently, important features are extracted from the tumor sequence using the

LSTM and passed as input to the GAN. The generator uses the LSTM's output to construct the 3D reconstruction, while the discriminator distinguishes between the generated and real images. The proposed approach is tested and evaluated using the commonly used LUNA dataset. The LUNA dataset has been extensively used in lung cancer diagnosis and is considered a standard benchmark for evaluating algorithms related to lung nodule detection and classification. It comprises more than 1,000 chest CT scans, with each scan annotated with multiple nodules. The main contributions are listed below:

- The majority of current approaches for reconstructing 3D tumors concentrate on brain cancer and do not yield satisfactory outcomes for lung cancer tumors. Accordingly, this study concentrates only on the 3D construction of tumors related to lung cancer.
- Afshar et al. [3] conducted the latest research on the reconstruction of lung cancer tumors, which has a relatively high level of computational complexity. However, the suggested technique surpasses Afshar's investigation in regards to effectiveness and computational intricacy.
- Although GAN has the potential to generate high-quality synthetic images, its application in medical diagnosis, particularly for lung cancer diagnosis, has been limited. This investigation seeks to examine the utilization of GAN in constructing three-dimensional lung tumor representations, which is a novel approach in the field.
- In the medical domain, it is frequently encountered to have insufficient labeled training data. To address this, pre-trained models (transfer learning) are often used.
- Reconstructing 3D images of lung cancer tumors involves using a series of 2D CT images. To exploit the sequential nature of this information, recurrent neural networks such as LSTM are utilized.

The paper is structured in the following manner: Section II discusses related work, Section III details the suggested methodology, while Section IV displays the experimental findings, and Section V discusses the results. Section VI concludes the paper and provides future directions.

II. RELATED WORK

A. Generative Adversarial Network

Liao et al. [18] utilized incorrect sampling to reconstruct cone beam CT (CBCT). The model involved the utilization of pyramidal neural networks and computer-generated maps for descriptive discriminants. This approach enabled the reconstruction of results while simultaneously preserving the anatomical structure. MR image reconstruction evaluates k-space data in the frequency domain model. Different loss functions have been employed to identify localized image structures in image restoration, such as coherence loss and cycle consistency loss, when suppressing cardiac CT noise. Wolterink et al. [19] proposed a low-dose CT noise after attenuation of losses in several areas. However, the result prevented the projection of the local image. MRI image

reconstructions are uncommon because they have well-defined back-and-forth formulas such as Fourier transforms.

B. Pre-trained Model

More training data leads to deep models with better performance [20]. That is why significant efforts have been put into gathering and annotating large-scale datasets such as ImageNet, PASCAL VOC, MS COCO, etc [21]. At the start of training, setting the initial parameters of deep models to the parameters of deep models that have already been trained on these large datasets improves the convergence speed of training. It boosts the final performance of the model [22].

3D semantic segmentation is quite common in the medical domain. For example, small organ segmentation in 3D abdominal CT scans has been tackled using an RNN [23]. Most medical 3D image analyses, including [24], train a deep model from scratch, which is challenging due to insufficient annotated data. Alternatively, the model's parameters can be initialized to values pre-trained on a source dataset. The model can then be fine-tuned using (possibly limited) target dataset. To get reasonable results, the distribution of the source and target datasets should be as similar as possible [25]. Therefore, for training deep models on 3D medical images, the model should be initialized to values pre-trained on another 3D medical dataset.

C. 3D Tumor Reconstruction

Lately, 3D models have been created in various medical areas, allowing doctors to provide improved treatment to their patients [26-28]. For example, 3D models were applied to liver resection, assisting surgeons in studying the liver structure [29]. 3D reconstruction of the brain based on magnetic resonance imaging (MRI) [30, 31] has been tackled as well [32, 33]. Amruta et al. [34] proposed a 3D method for brain tumor recovery in which brain tumors were segmented by morphological manipulations and 3D shapes were generated using 3D interpolation. Jaffar et al. [35] considered a multi-step process for segmenting and visualizing brain tumors evaluated on different datasets. Kamencay et al. [36] used the medium screening method to segment the images. For modeling the 3D shape, a combination of the Sum of Squared Differences (SSD) and Speeded-Up Robust Features (SURF) was used to find the corresponding pixels in the image. The method provides an accurate 3D model of the human pelvis. Sun et al. [37] proposed a two-step 3D segmentation that involves identifying active shape models and finding the optimal surface. Several studies have developed valuable methods to address 3D tumor reconstruction [38].

In the context of lung cancer, Afshar et al. [3] recently proposed a method for tumor segmentation and 3D reconstruction of CT images. While this is a significant step towards improving lung cancer treatment, the method has a high computational complexity. This drawback limits its practical applications and motivates the development of new approaches with improved performance and reduced computational costs. Therefore, this study aims to explore a novel approach using GAN for 3D reconstruction of lung cancer tumors, which can potentially overcome the limitations of existing methods.

III. THE PROPOSED MODEL

GANs were first proposed by Goodfellow et al. [39], in which two separate networks are similarly trained: the generator and discriminator networks. The purpose of the generator is to produce data such as images, text, etc. [40], which are structurally similar to real data but are fake. On the other hand, the task of the discriminator network is to strengthen the generator. These two networks engage in a two-player min-max game with a value function $V(D,G)$ [41]:

$$\begin{aligned} \min_G \max_D V(D,G) \\ = E_{x \sim p_{data}(x)} [\log(D(x))] \\ + E_{z \sim p_z(z)} [\log(1 \\ - D(G(z)))] \end{aligned} \quad (1)$$

where x and z represent input data and noise, respectively. G and D denote the generator and discriminator, respectively. $p_{data}(x)$ and $p_z(z)$ show the probability distributions of the input data and the noise, respectively. E represents mathematical expectation.

The objective is to evaluate the 3D morphology of lung tumors using a limited set of 2D CT images. The general outline for the suggested model is presented in Fig. 1. Based on this illustration, the model comprises three stages, namely lung partitioning, tumor partitioning, and 3D rebuilding. Using the snake optimization method, lung segmentation aims to separate two lungs from a CT image. In the tumor localization phase, the region of the tumor in the lung is identified from the healthy region on each 2D slice using snake optimization and GK clustering. Then, a GAN-based model is utilized to reconstruct the 3D model of the tumor. The following sections will be described separately.

A. Lung Segmentation

Segmentation of the lungs is a vital stage in the task and can influence the model's efficacy considerably. The method used for lung segmentation was adopted from a recent study [42].

The approach involves using the snake optimization method to separate the lungs from the background. This method allows the lung outline of one section to serve as the initial outline for subsequent sections in the algorithm [43]. The snake model refers to a curve that starts at a specific point and then moves towards the boundaries of an object. This procedure is referred to as a semi-automated process since it requires some degree of user involvement. This article uses the point-based snake model, which considers a contour as a collection of distinct points, although there are various snake models available [44]. The procedure aims to reduce an energy function [45, 46] that includes internal and external energies, where the internal energy is associated with the form of the contour. On the other hand, external energy relies on image characteristics. Given coordinates $x(s)$ and $y(s)$ in the direction of the contour, where s is a variable between zero and one, the contour can be defined in the following way [47]:

$$v(s) = [x(s), y(s)] \quad (2)$$

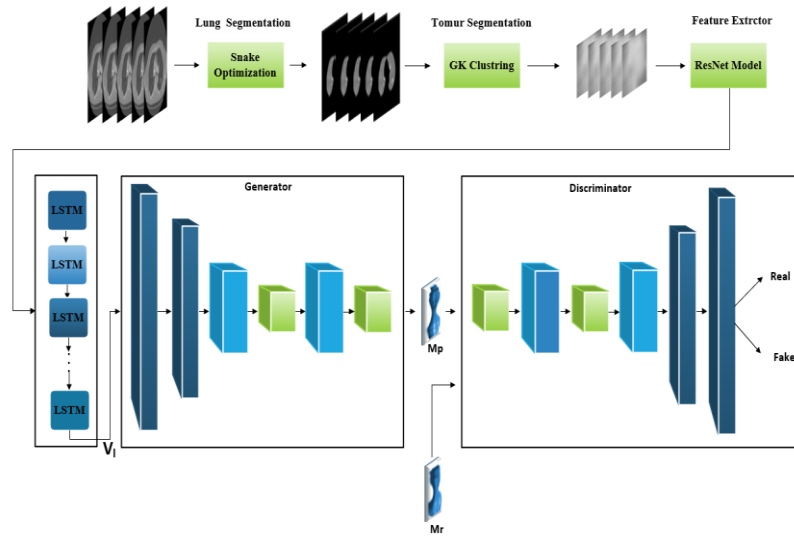


Fig. 1. The proposed model.

Where $v(s)$ represents the snake curve variable, the energy function is defined as follows:

$$E_{snake}^* = \int_0^1 E_{snake}^*(v(s)) ds \quad (3)$$

$$= \int_0^1 (E_{int}(v(s)) + E_{image}(v(s)) + E_{con}(v(s))) ds$$

where E_{con} indicates constant external forces. E_{int} and E_{image} denote the internal energy and the image forces, correspondingly, which can be calculated as:

$$E_{int} = \alpha(s) \left(\frac{dv}{ds}\right)^2 + \beta(s) \left(\frac{d^2s}{dv^2}\right)^2 \quad (4)$$

$$E_{image} = -|\nabla I(x, y)|^2 \quad (5)$$

The initial term turns the snake into a membrane. Increasing the value of β results in an increase in the internal energy, while the image energy comprises the energy of edge, line, and terminations. The value of $I(x, y)$ corresponds to the intensity of the pixel located at (x, y) . The negative sign at the beginning of Equation 5 is utilized since the image gradient is more prominent on the object boundary, and the objective of energy minimization is to detect the object boundary. The aim of the energy function with the damping term is to detect object boundaries. The Viterbi algorithm [48], a widely used technique for optimizing energy functions, is used in this study.

B. Tumor Segmentation

After the lung segmentation stage, tumors are segmented utilizing the GK clustering method. GK is a fuzzy-based approach with the benefits of using covariance and distance matrixes to make clusters with various shapes. The objective function of this method is defined as follows:

$$J_m(U, A_k) = \sum_{i=1}^M \sum_{k=1}^K u_{ik}^2 D^2_{ikA_k} \quad (6)$$

Where U stands for the membership matrix, and m is a coefficient describing the degree of fuzziness. A_k shows a regional norm-inducing matrix for each cluster optimized. M and K are the number of data points and clusters, respectively, and D^2 indicates the squared space between data points and cluster centers., which is calculated as:

$$D^2_{ikA_k} = (z_i - w_k)^T A_k (z_i - w_k) \quad (7)$$

The matrix is used to incorporate the topological characteristics of the data structure into the distance norm.

C. 3D Reconstruction Method

In this paper, 3D reconstruction is carried out using a deep learning model. As shown in Fig. 1, the tumor segmentation stage yields N sequences of 2D images. These images are fed to the pre-trained ResNet network to perform feature extraction. The parameters of this network have been determined by training on the ImageNet dataset. The output of the ResNet is used as input to LSTM units, the output of which is fed to a GAN model. GAN aims to reconstruct 3D images from sequences of 2D data fed to it. The GAN discriminator distinguishes between the synthetic images produced by the generator and the real ones.

D. Overall Algorithm

The overall algorithm of the suggested method is displayed in Algorithm 1. Let $Pateints = \{P^1, P^2, P^3, \dots, P^N\}$ be the set of available patients with N examples, where P^i corresponds to the i -th patient. Every P^i contains a collection of S CT images. In every iteration, for every minibatch with size M , the lung segmentation and tumor segmentation operations are performed, respectively. After that, the sequence of selected lung tumors for every patient whose length is L enters the ResNet model. The L -sample sequence outputted by ResNet is fed into an LSTM. Finally, LSTM output comes into the generator to generate a 3D lung tumor. Updating the components, i.e., LSTM, generator, and discriminator, is done based on introduced standard methods.

Algorithm 1 Overall algorithm for the suggested model.

Input: $Pateints = \{P^1, P^2, P^3, \dots, P^N\}$: the set of available patients, $Images = \{X^1, X^2, X^3, \dots, X^N\}$: the set of available real 3D images, N : the number of patients, S : the number of CT images for every patient, G : generator, D : discriminator;
 for the number of training iterations, do
 for every minibatch with size M do
 for $i = 1$ to M do
 for $j = 1$ to S do
 P_t^{ij} : segment P^{ij} using the snake algorithm; // P^{ij} shows the j -th CT image for the i -th patient
 for $i = 1$ to M do
 $\{P_t^{i1}, P_t^{i2}, P_t^{i3}, \dots, P_t^{iL}\}$: select $L(\leq S)$ consecutive samples containing tumors recognized by the GK clustering from
 $\{P_v^{i1}, P_v^{i2}, P_v^{i3}, \dots, P_v^{iL}\}$;
 $\{P_v^{i1}, P_v^{i2}, P_v^{i3}, \dots, P_v^{iL}\}$: extract features every item of $\{P_t^{i1}, P_t^{i2}, P_t^{i3}, \dots, P_t^{iL}\}$ using the ResNet model;
 V_v^i : enter $\{P_v^{i1}, P_v^{i2}, P_v^{i3}, \dots, P_v^{iL}\}$ into the LSTM network and get the latest unit of LSTM;
 update the LSTM network by its stochastic gradient;
 update the generator by descending its stochastic gradient:
 $\nabla_{\theta_g} \frac{1}{M} \sum_{i=1}^M \log(1 - D(g(V_v^i)))$
 Update the discriminator by ascending its stochastic gradient:
 $\nabla_{\theta_d} \frac{1}{M} \sum_{i=1}^M [\log D(x^i) + \log(1 - D(g(V_v^i)))]$

IV. EMPIRICAL EVALUATION

A. Dataset

The suggested method was evaluated using the LUNA subset of a dataset (referred to as LIDA-IDRI) [49]. The LIDA-IDRI is a lung CT scan public dataset, which includes 220 patients with more than 130 slices. The LUNA 2016 dataset was designed to analyze lung nodules and received 888 CT scans with a section thickness of less than 3 mm and 512×512 pixels picture size. The node has a total of 36,378 notes annotated by various radiologists. However, nodes 2290, 1602, 1186, and 777 are annotated by radiologists 1, 2, 3, and 4, respectively. Node annotations approved by at least three radiologists are called valid annotations. Diameter and position annotations are average annotations in LIDA-IDRI. The LUNA dataset originally was not a 3D image, so the 3D image was created manually using Rhinoceros 3D software.

B. Lung Segmentation and Tumor Detection

The lung and surrounding area have been isolated from the images utilising snake optimization. The method was contrasted with fuzzy-based techniques, namely FCM [50], KFCM [51], SAFCM [52], and FRFCM [53]. The evaluation was based on the metrics of Intersection over Union (IoU) [54] and Hausdorff distance [55], and the results are shown in Table I. The FRFCM method performed better than SAFCM and KFCM, with an improvement of approximately 20% and 13%, respectively. However, even though FRFCM is considered a robust algorithm, it still does not match the performance of Snake. The Snake algorithm showed a 22% improvement in the IoU metric compared to FRFCM. Examples of lungs delineated using the Snake algorithm are shown in Fig. 2.

Following the segmentation of lungs with the Snake algorithm, clustering methods including FCM, K-means, and GK were employed to create two clusters for lung tumor segmentation. Evaluation was carried out using the IoU and HD metrics, and the results are presented in Table II. According to the table, GK clustering is the most effective method for segmenting lung tumors. Lung cancers can also be segmented using FCM and K-means clustering, as shown in the table. Fig. 3 illustrates examples of tumor detection with the GK clustering technique.

TABLE I. EVALUATION OF THE SEGMENTATION EFFICIENCY OF DIFFERENT FUZZY ALGORITHMS

Method	IoU	HD
FCM	0.621	1.496
KFCM	0.746	1.715
SAFCM	0.721	1.852
FRFCM	0.785	2.019
Snake	0.831	2.151

TABLE II. ANALYSIS OF THE PROPOSED MODEL IN COMPARISON TO PREVIOUS WORKS

Method	IoU	HD
FCM	0.751	2.122
K-mean	0.780	1.615
GK	0.786	1.419

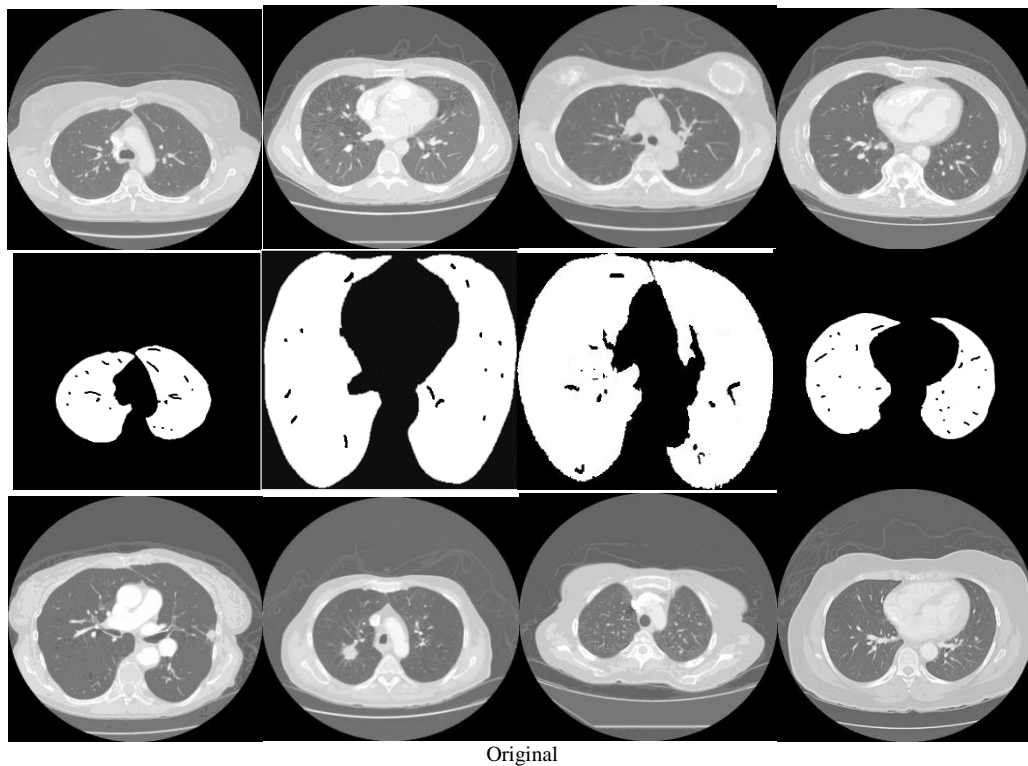


Fig. 2. The instances of lungs that were segmented using the snake algorithm.

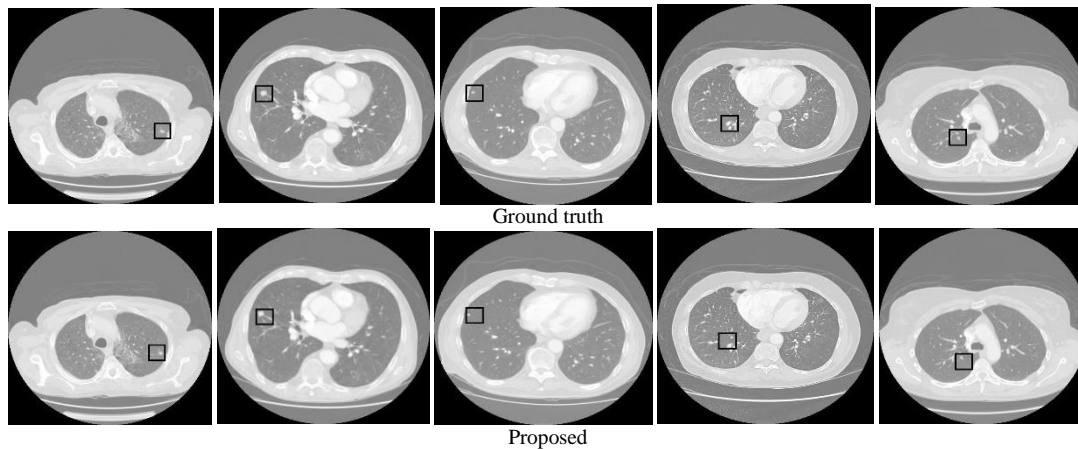


Fig. 3. The samples of identifying tumors using the GK method.

C. 3D Reconstruction

The evaluation of the 3D reconstruction model included comparing four different methods: MC [56], MC and fairing [57], interpolation [34], and MC, and Afshar et al. [3]. The evaluation metrics used were HD and ED, which measured shape accuracy and pixel-wise distance, respectively. The results of the evaluation are presented in Table III, where MC performed the worst with values of 8.50 and 3.21 for HD and ED, respectively. However, the addition of fairing to MC decreased the values to 6.82 and 2.99. Interpolation with MC further reduced the error by approximately 0.555 and 0.855 for the two metrics, respectively. Despite these improvements, the recent work of Afshar et al. outperformed all other methods, including MC and MC + fairing, with values of 5.39 and 1.45

for HD and ED, respectively. Interestingly, the proposed model, which uses a strong GAN to create 3D shapes, outperformed Afshar et al.'s method, even though they had similar lung segmentation and tumor detection. The difference in performance may be attributed to the nature of the methods, as the proposed model relies on GANs, which have proven to be effective in generating complex data distributions. On the other hand, other methods use mathematical operations to create 3D shapes, which may not capture the underlying complexity of the data as well as GANs. In conclusion, the proposed model with a strong GAN is a promising approach for accurate 3D reconstruction, especially for complex medical imaging data.

TABLE III. THE EVALUATION AND COMPARISON OF THE SUGGESTED APPROACH WITH OTHER EXISTING METHODS

Model	HD	ED
MC	8.50	3.21
MC+ fairing	6.82	2.99
Interpolation + MC	5.85	2.57
Afshar et al. [3]	5.39	1.45
Proposed	2.99	1.06

Table IV demonstrates that the model is effective in accurately reconstructing 3D shapes from the provided input images. The reconstructed shapes closely resemble the original ones, and the input images are smooth, which is critical for accurate medical diagnoses. The smoothness issue faced by other methods can lead to incorrect diagnoses, and the generated images by these methods do not resemble the

original ones. The proposed model has successfully addressed these issues, demonstrating its superiority over other methods. Table V shows the computational efficiency of the suggested model and other approaches. The traditional methods take more time because of their lower computational efficiency. Nonetheless, the ResNet model, which is utilized for image recognition, consumes the most time in the proposed model. Despite this, the proposed model still outperforms other methods that use heavy computational operations, indicating its superiority in terms of accuracy and computational efficiency trade-off compared to existing methods. The results suggest that the proposed model has great potential for real-world medical applications. Its ability to generate smooth and accurate 3D images can help physicians make more precise diagnoses, which can lead to improved patient outcomes. Additionally, the model's computational efficiency makes it suitable for use in clinical settings where time is a critical factor.

TABLE IV. CREATED 3D SHAPES RESEMBLING TUMORS

Original	MC	MC+ fairing	Interpolation + MC	Afshar et al.	Proposed
					
					
					
					
					
					
					

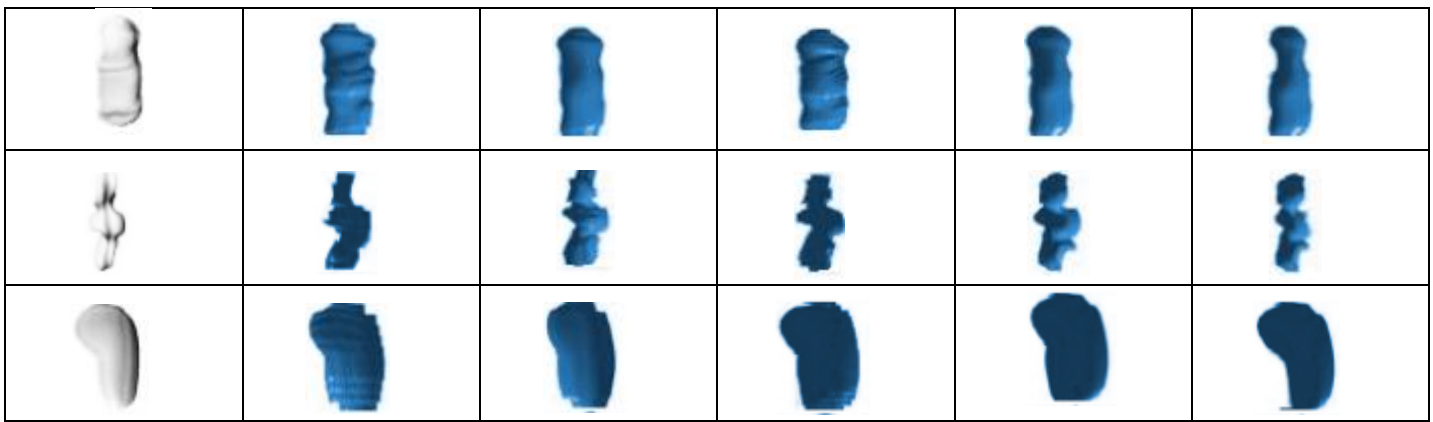


TABLE V. THE DURATION OF TIME TAKEN BY ALGORITHMS TO EXECUTE (IN MILLISECONDS)

Image \ Model	MC	MC+ fairing	Interpolation + MC	Afshar et al.	Proposed
1	506	496	435	408	351
2	475	527	498	449	410
3	365	336	279	319	230
4	614	595	591	585	563
5	651	639	626	574	480
6	720	661	705	680	621
7	561	538	477	499	425
8	741	729	742	691	670
9	481	507	489	452	430
10	558	579	578	539	500

1) *Analysis of pre-trained models:* The experiments carried out in this research demonstrate the superiority of the ResNet model compared to other pre-trained models, namely AlexNet [58], GoogleNet [59], Inceptionv3 [60], DenseNet [61], and MobileNet [62] (refer Table VI). Although other models have been extensively utilized in diverse image recognition works, they cannot match the ResNet model's performance in 3D reconstruction. The ResNet model significantly outperforms the other models, leading to a remarkable improvement in the HD and ED error metrics. These results highlight the importance of selecting an appropriate pre-trained model for achieving optimal performance in 3D reconstruction. Thus, the experimental findings provide solid evidence for the use of the ResNet model as the feature extractor in the suggested model.

2) *Explore the hidden size:* The LSTM network's hidden vector serves as a practical tool to compress data from a sequence of 2D images and aid in drawing 3D shapes. Increasing the hidden size can add more data to the model, but it may not always be useful. A limited capacity of the hidden size is inadequate to store the required data. Eight different values ranging from 16 to 2056 were evaluated to explore the influence of the hidden dimension on the suggested model. The outcomes are depicted in Fig. 4. Upon examination, it was observed that for HD and ED, the chart shows a descending trend when the hidden size is within the range of [16, 128], and an ascending trend from [128, 2056]. As a result, the optimal hidden size is 128.

3) *Analysis of loss function:* Selecting an appropriate loss function is vital for the success of deep learning models, as neglecting it may cause the model to be trapped in local optima. Therefore, the study aimed to assess how the discriminator's performance was affected by various loss functions. Five functions were selected for this purpose, namely Weighted Cross-Entropy (WCE) [63], Balanced Cross-Entropy (BCE) [64], Dice Loss (DL) [65], Tversky Loss (TL) [66], and Sensitivity Specificity Loss (SSL) [67]. WCE is a modified version of BCE that assigns different weights to examples from one class. Even though DL was originally developed to compare two images, it has been suggested as a loss function. The outcomes of these loss functions are presented in a tabular format in Table VII. Among the examined loss functions, TL exhibited the most superior performance, attaining an ED of 1.06 and an HD of 3.02. Although WCE assigns weights to the samples, TL still outperformed it, improving the error of WCE by approximately 1.64 and 2.50.

TABLE VI. THE RESULTS OBTAINED FOR USING VARIOUS PRE-TRAINED MODELS

Model	HD	ED
AlexNet	3.49	1.98
GoogleNet	4.85	3.11
Inceptionv3	4.19	2.51
DenseNet	6.46	3.79
MobileNet	6.84	4.93

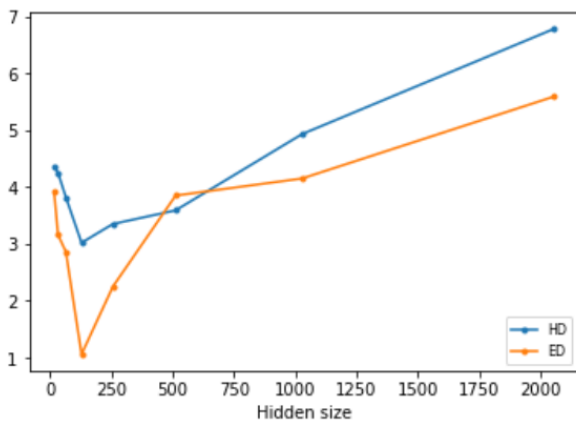


Fig. 4. The HD and ED performance metrics plot corresponding to different units in hidden layers.

TABLE VII. THE OUTCOMES ACHIEVED WITH VARIOUS DISCRIMINATOR LOSS FUNCTIONS

Loss function	HD	ED
WCE	4.58	3.49
BCE	3.80	3.16
DL	3.59	2.69
TL	3.09	1.08
SSL	3.32	2.15

V. DISCUSSION

The study's proposed approach for 3D lung tumor reconstruction using deep learning techniques offers promising results for medical diagnosis applications. The superior performance compared to traditional approaches on the LUNA dataset demonstrates the potential of deep learning techniques in the diagnosis and treatment of lung cancer. However, the study also highlights several limitations that should be addressed in future work.

One major limitation of the proposed method is the relatively small size of the LUNA dataset, which may limit the model's generalizability. Therefore, future studies could focus on expanding the dataset size to validate the proposed method's effectiveness on a larger scale. Additionally, incorporating other imaging modalities, such as PET scans, could improve the accuracy of the lung tumor reconstruction. Furthermore, the proposed method's generalizability to different datasets and populations should be thoroughly investigated in future studies to assess its practicality in clinical settings. The evaluation of the proposed method was done only on the LUNA dataset, and further evaluation on other datasets would be necessary to validate its performance. Additionally, the proposed method requires a large amount of labeled data for training, and the scarcity of such data in medical imaging remains a challenge. Therefore, further studies could focus on developing techniques for efficient data labeling to improve the availability of labeled data. Lastly, the interpretability of the proposed model could be improved. While the model can generate 3D lung tumor images, it is not always clear how the model arrived at a particular result. Future work could explore ways to make the model more interpretable, such as using attention mechanisms or visualization techniques. This could help

increase the transparency of the model's decision-making process and improve trust among clinicians and patients.

In addition to the limitations discussed earlier, there are also other aspects of the proposed method that could be improved in future work. For instance, the proposed method involves several complex steps, including lung isolation, tumor detection, and 3D lung tumor re-creation. Each of these steps requires careful tuning of hyperparameters and may introduce errors that can affect the overall performance of the model. Therefore, future studies could explore ways to simplify the proposed method by combining some of these steps or using alternative segmentation methods. Moreover, the proposed method assumes that the lung tumor is visible in the input image, which may not always be the case. For instance, small tumors or tumors that are located close to other organs may be challenging to detect using the proposed method. Therefore, future studies could explore ways to incorporate other features, such as patient history or genetic information, to improve the model's sensitivity and specificity. Another disadvantage of the suggested method is the computational cost, which may limit its practicality in clinical settings. While the proposed method shows promising results, it requires substantial computational resources, including high-end GPUs and extensive training time. Therefore, future studies could focus on developing more efficient models that can achieve similar performance with fewer computational resources. Lastly, the ethical implications of the proposed method should also be taken into account in future research. Deep learning models can be used to make critical medical decisions, and it is crucial to ensure that such models are fair and unbiased. Therefore, future studies could explore ways to ensure that the proposed method does not reinforce existing biases or discriminate against certain patient populations.

VI. CONCLUSION

The study proposes a novel method for constructing 3D lung tumors, which combines an LSTM and GAN network with a ResNet model serving as the feature extractor. The technique is divided into three stages: lung isolation, tumor isolation, and 3D lung tumor reconstruction. To achieve lung isolation and tumor isolation, the snake optimization and GK techniques are employed. In the 3D reconstruction phase, the pre-trained ResNet model is used to extract features from 2D lung tumor images, followed by the provision of these features into an LSTM to produce compressed features. The compressed characteristics are then utilized as input for GAN, where the generator is accountable for producing 3D lung tumor images, and the discriminator ascertains the authenticity of the image. The suggested model is evaluated on the LUNA dataset, and standard evaluation metrics are used to compare its effectiveness with conventional techniques.

One potential future work based on this study could be to investigate the proposed technique's applicability to other types of cancer or medical imaging modalities. It would be interesting to see how the proposed model could be adapted and optimized to handle different types of tumors, such as those found in breast or prostate cancer. Additionally, exploring the potential of incorporating other deep learning architectures or loss functions could further enhance the

accuracy and efficiency of the proposed method. Finally, conducting a clinical validation study to assess the proposed model's usefulness in real-world settings would be a valuable next step towards its eventual clinical adoption.

FUNDING

This work was supported by the Humanities and Social Sciences Project of Henan Provincial Education Department (No. 2022-ZZJH-098), the Graduate Quality Engineering Project of Zhongyuan University of Technology (No. QY202102), and the Advantageous Disciplines Strength Improvement Project of Zhongyuan University of Technology (No. 2022001).

REFERENCES

- [1] R. Raja, S. Kumar, S. Rani, K.R. Laxmi, Lung segmentation and nodule detection in 3D medical images using convolution neural network, *Artificial Intelligence and Machine Learning in 2D/3D Medical Image Processing*, CRC Press 2020, pp. 179-188.
- [2] J. Zhou, H. Xin, Emerging artificial intelligence methods for fighting lung cancer: A survey, *Clinical eHealth*, 5, pp. 19-34, 2022.
- [3] P. Afshar, A. Ahmadi, A. Mohebi, M. Fazel Zarandi, A hierarchical stochastic modelling approach for reconstructing lung tumour geometry from 2D CT images, *Journal of Experimental & Theoretical Artificial Intelligence*, 30, pp. 973-992, 2018.
- [4] A. Ashraf, S. Naz, S.H. Shirazi, I. Razzak, M. Parsad, Deep transfer learning for alzheimer neurological disorder detection, *Multimedia Tools and Applications*, 80, pp. 30117-30142, 2021.
- [5] X. Yi, E. Walia, P. Babyn, Generative adversarial network in medical imaging: A review, *Medical image analysis*, 58, pp. 101552, 2019.
- [6] R. Wang, Z. Fang, J. Gu, Y. Guo, S. Zhou, Y. Wang, C. Chang, J. Yu, High-resolution image reconstruction for portable ultrasound imaging devices, *EURASIP Journal on Advances in Signal Processing*, 2019, pp. 1-12, 2019.
- [7] G. Yang, S. Yu, H. Dong, G. Slabaugh, P.L. Dragotti, X. Ye, F. Liu, S. Arridge, J. Keegan, Y. Guo, DAGAN: deep de-aliasing generative adversarial networks for fast compressed sensing MRI reconstruction, *IEEE transactions on medical imaging*, 37, pp. 1310-1321, 2017.
- [8] S.V. Moravvej, S.J. Mousavirad, D. Oliva, G. Schaefer, Z. Sobhaninia, An Improved DE Algorithm to Optimise the Learning Process of a BERT-based Plagiarism Detection Model, 2022 IEEE Congress on Evolutionary Computation (CEC), IEEE, pp. 1-7, 2022.
- [9] M.S. Sartakhti, M.J.M. Kahaki, S.V. Moravvej, M. javadi Joortani, A. Bagheri, Persian language model based on BiLSTM model on COVID-19 corpus, 2021 5th International Conference on Pattern Recognition and Image Analysis (IPRIA), IEEE, pp. 1-5, 2021.
- [10] S.V. Moravvej, M.J.M. Kahaki, M.S. Sartakhti, A. Mirzaei, A method based on attention mechanism using bidirectional long-short term memory (BLSTM) for question answering, 2021 29th Iranian Conference on Electrical Engineering (ICEE), IEEE, pp. 460-464, 2021.
- [11] S.V. Moravvej, M. Joodaki, M.J.M. Kahaki, M.S. Sartakhti, A method Based on an Attention Mechanism to Measure the Similarity of two Sentences, 2021 7th International Conference on Web Research (ICWR), IEEE, pp. 238-242, 2021.
- [12] S.V. Moravvej, S.J. Mousavirad, M.H. Moghadam, M. Saadatmand, An lstm-based plagiarism detection via attention mechanism and a population-based approach for pre-training parameters with imbalanced classes, *Neural Information Processing: 28th International Conference, ICONIP 2021, Sanur, Bali, Indonesia, December 8-12, 2021, Proceedings, Part III 28*, Springer, pp. 690-701, 2021.
- [13] M. Jiang, M. Zhi, L. Wei, X. Yang, J. Zhang, Y. Li, P. Wang, J. Huang, G. Yang, FA-GAN: Fused attentive generative adversarial networks for MRI image super-resolution, *Computerized Medical Imaging and Graphics*, 92, p. 101969, 2021.
- [14] H.-C. Shin, N.A. Tenenholtz, J.K. Rogers, C.G. Schwarz, M.L. Senjem, J.L. Gunter, K.P. Andriole, M. Michalski, Medical image synthesis for data augmentation and anonymization using generative adversarial networks, *Simulation and Synthesis in Medical Imaging: Third International Workshop, SASHIMI 2018, Held in Conjunction with MICCAI 2018, Granada, Spain, September 16, 2018, Proceedings 3*, Springer, pp. 1-11, 2018.
- [15] P.V. Klimov, J. Kelly, J.M. Martinis, H. Neven, The snake optimizer for learning quantum processor control parameters, *arXiv preprint arXiv:2006.04594*, 2020.
- [16] F.A. Hashim, A.G. Hussien, Snake Optimizer: A novel meta-heuristic optimization algorithm, *Knowledge-Based Systems*, p. 108320, 2022.
- [17] D. Dovžan, I. Škrjanc, Recursive clustering based on a Gustafson-Kessel algorithm, *Evolving systems*, 2, pp. 15-24, 2011.
- [18] H. Liao, Z. Huo, W.J. Sehnert, S.K. Zhou, J. Luo, Adversarial sparse-view CBCT artifact reduction, *International Conference on Medical Image Computing and Computer-Assisted Intervention*, Springer, pp. 154-162, 2018.
- [19] J.M. Wolterink, T. Leiner, M.A. Viergever, I. Išgum, Generative adversarial networks for noise reduction in low-dose CT, *IEEE transactions on medical imaging*, 36, pp. 2536-2545, 2017.
- [20] C. Sun, A. Shrivastava, S. Singh, A. Gupta, Revisiting unreasonable effectiveness of data in deep learning era, *Proceedings of the IEEE international conference on computer vision*, pp. 843-852, 2017.
- [21] A. Karimi, S.M.R. Hashemian, Cytokine storm in COVID-19 and the treatment simulacrum, *Biomedical and Biotechnology Research Journal (BBRJ)*, 4, p. 41, 2020.
- [22] O. Russakovsky, J. Deng, H. Su, J. Krause, S. Satheesh, S. Ma, Z. Huang, A. Karpathy, A. Khosla, M. Bernstein, Imagenet large scale visual recognition challenge, *International journal of computer vision*, 115, pp. 211-252, 2015.
- [23] Q. Yu, L. Xie, Y. Wang, Y. Zhou, E.K. Fishman, A.L. Yuille, Recurrent saliency transformation network: Incorporating multi-stage visual cues for small organ segmentation, *Proceedings of the IEEE conference on computer vision and pattern recognition*, pp. 8280-8289, 2018.
- [24] X. Han, Automatic liver lesion segmentation using a deep convolutional neural network method, *arXiv preprint arXiv:1704.07239*, 2017.
- [25] H. Nam, B. Han, Learning multi-domain convolutional neural networks for visual tracking, *Proceedings of the IEEE conference on computer vision and pattern recognition*, pp. 4293-4302, 2016.
- [26] S. AlZu'bi, Y. Jararweh, H. Al-Zoubi, M. Elbes, T. Kanan, B. Gupta, Multi-orientation geometric medical volumes segmentation using 3d multiresolution analysis, *Multimedia Tools and Applications*, 78, pp. 24223-24248, 2019.
- [27] S. Al-Zu'bi, B. Hawashin, A. Mughaid, T. Baker, Efficient 3D medical image segmentation algorithm over a secured multimedia network, *Multimedia Tools and Applications*, 80, pp. 16887-16905, 2021.
- [28] A.A. Albishri, S.J.H. Shah, S.S. Kang, Y. Lee, AM-UNet: automated mini 3D end-to-end U-net based network for brain claustrum segmentation, *Multimedia Tools and Applications*, pp. 1-24, 2022.
- [29] R. Palomar, F.A. Cheikh, B. Edwin, A. Beghdadhi, O.J. Elle, Surface reconstruction for planning and navigation of liver resections, *Computerized Medical Imaging and Graphics*, 53, pp. 30-42, 2016.
- [30] S. Danaei, A. Bostani, S.V. Moravvej, F. Mohammadi, R. Alizadehsani, A. Shoeibi, H. Alinejad-Rokny, S. Nahavandi, Myocarditis Diagnosis: A Method using Mutual Learning-Based ABC and Reinforcement Learning, 2022 IEEE 22nd International Symposium on Computational Intelligence and Informatics and 8th IEEE International Conference on Recent Achievements in Mechatronics, Automation, Computer Science and Robotics (CINTI-MACRO), IEEE, pp. 000265-000270, 2022.
- [31] S.V. Moravvej, R. Alizadehsani, S. Khanam, Z. Sobhaninia, A. Shoeibi, F. Khozeimeh, Z.A. Sani, R.-S. Tan, A. Khosravi, S. Nahavandi, RLMD-PA: a reinforcement learning-based myocarditis diagnosis combined with a population-based algorithm for pretraining weights, *Contrast Media & Molecular Imaging*, 2022, 2022.
- [32] S. Momin, Y. Lei, Z. Tian, J. Roper, J. Lin, S. Kahn, H.-K. Shu, J.D. Bradley, T. Liu, X. Yang, Cascaded Mutual Enhancing Networks for Brain Tumor Subregion Segmentation in Multiparametric MRI, *Physics in Medicine & Biology*, 2022.

- [33] B. Yang, L. Zhou, L. Chen, L. Lu, H. Liu, W. Zhu, Cycle-consistent learning-based hybrid iterative reconstruction for whole-body PET imaging, *Physics in Medicine & Biology*, 2022.
- [34] A. Amruta, A. Gole, Y. Karunakar, A systematic algorithm for 3-D reconstruction of MRI based brain tumors using morphological operators and bicubic interpolation, 2010 2nd International Conference on Computer Technology and Development, IEEE, pp. 305-309, 2010.
- [35] M.A. Jaffar, S. Zia, G. Latif, A.M. Mirza, I. Mehmood, N. Ejaz, S.W. Baik, Anisotropic diffusion based brain MRI segmentation and 3D reconstruction, *International Journal of Computational Intelligence Systems*, 5, pp. 494-504, 2012.
- [36] P. Kamencay, M. Zachariasova, R. Hudec, M. Benco, R. Radil, 3D image reconstruction from 2D CT slices, 2014 3DTV-Conference: The True Vision-Capture, Transmission and Display of 3D Video (3DTV-CON), IEEE, pp. 1-4, 2014.
- [37] S. Sun, C. Bauer, R. Beichel, Automated 3-D segmentation of lungs with lung cancer in CT data using a novel robust active shape model approach, *IEEE transactions on medical imaging*, 31, pp. 449-460, 2011.
- [38] S.M. Ganji, M. Tehrani, A. Ehterami, H. Semyari, F. Taleghani, M. Habibzadeh, M.H. Tayeed, N. Mehrnia, A. Karimi, M. Salehi, Bone tissue engineering via application of a PCL/Gelatin/Nanoclay/Hesperetin 3D nanocomposite scaffold, *Journal of Drug Delivery Science and Technology*, 76, p. 103704, 2022.
- [39] I. Goodfellow, J. Pouget-Abadie, M. Mirza, B. Xu, D. Warde-Farley, S. Ozair, A. Courville, Y. Bengio, Generative adversarial nets, *Advances in neural information processing systems*, 27, 2014.
- [40] S. Moravvej, M. Maleki Kahaki, M. Salimi Sartakhti, M. Joodaki, Efficient GAN-based Method for Extractive Summarization, *Journal of Electrical and Computer Engineering Innovations (JECEI)*, 2021.
- [41] S.V. Moravvej, A. Mirzaei, M. Safayani, Biomedical text summarization using Conditional Generative Adversarial Network (CGAN), *arXiv preprint arXiv:2110.11870*, 2021.
- [42] P. Afshar, A. Ahmadi, M.F. Zarandi, Lung tumor area recognition in CT images based on Gustafson-Kessel clustering, 2016 IEEE International Conference on Fuzzy Systems (FUZZ-IEEE), IEEE, pp. 2302-2308, 2016.
- [43] M.S. Hakemi, A.A. Nassiri, A. Nobakht, M. Mardani, I.A. Darazam, M. Parsa, M.M. Miri, R. Shahrami, A.A. Koomleh, K. Entezarmahdi, Benefit of hemoabsorption therapy in patients suffering sepsis-associated acute kidney injury: a case series, *Blood Purification*, 51, pp. 823-830, 2022.
- [44] T. Yona, Y. Or, The wheeled three-link snake model: singularities in nonholonomic constraints and stick-slip hybrid dynamics induced by Coulomb friction, *Nonlinear Dynamics*, 95, pp. 2307-2324, 2019.
- [45] S. Vakilian, S.V. Moravvej, A. Fanian, Using the artificial bee colony (ABC) algorithm in collaboration with the fog nodes in the Internet of Things three-layer architecture, 2021 29th Iranian Conference on Electrical Engineering (ICEE), IEEE, pp. 509-513, 2021.
- [46] S. Vakilian, S.V. Moravvej, A. Fanian, Using the cuckoo algorithm to optimizing the response time and energy consumption cost of fog nodes by considering collaboration in the fog layer, 2021 5th International Conference on Internet of Things and Applications (IoT), IEEE, pp. 1-5, 2021.
- [47] M. Sonka, V. Hlavac, R. Boyle, *Image processing, analysis, and machine vision*, Cengage Learning 2014.
- [48] N. Shlezinger, Y.C. Eldar, N. Farsad, A.J. Goldsmith, Viterbinet: Symbol detection using a deep learning based viterbi algorithm, 2019 IEEE 20th International Workshop on Signal Processing Advances in Wireless Communications (SPAWC), IEEE, pp. 1-5, 2019.
- [49] S.G. Armato III, G. McLennan, L. Bidaut, M.F. McNitt-Gray, C.R. Meyer, A.P. Reeves, B. Zhao, D.R. Aberle, C.I. Henschke, E.A. Hoffman, The lung image database consortium (LIDC) and image database resource initiative (IDRI): a completed reference database of lung nodules on CT scans, *Medical physics*, 38, pp. 915-931, 2011.
- [50] I.-D. Borlea, R.-E. Precup, A.-B. Borlea, D. Iercan, A unified form of fuzzy C-means and K-means algorithms and its partitional implementation, *Knowledge-Based Systems*, 214, p. 106731, 2021.
- [51] Y. Ding, X. Fu, Kernel-based fuzzy c-means clustering algorithm based on genetic algorithm, *Neurocomputing*, 188, pp. 233-238, 2016.
- [52] Q. Li, Z. Li, Z. Shi, H. Fan, Multi-Target Magnetic Positioning Using SAFCM Clustering and Invariants-Improved Tilt Angle, *IEEE Transactions on Geoscience and Remote Sensing*, 60, pp. 1-15, 2022.
- [53] Y. Shen, C. Tang, M. Xu, Z. Lei, Optical selective encryption based on the FRFCM algorithm and face biometric for the medical image, *Optics & Laser Technology*, 138, p. 106911, 2021.
- [54] H. Rezatofighi, N. Tsoi, J. Gwak, A. Sadeghian, I. Reid, S. Savarese, Generalized intersection over union: A metric and a loss for bounding box regression, *Proceedings of the IEEE/CVF Conference on Computer Vision and Pattern Recognition*, pp. 658-666, 2019.
- [55] J.M. Bogoya, A. Vargas, O. Schütze, The averaged hausdorff distances in multi-objective optimization: A review, *Mathematics*, 7, p. 894, 2019.
- [56] D. Luengo, L. Martino, M. Bugallo, V. Elvira, S. Särkkä, A survey of Monte Carlo methods for parameter estimation, *EURASIP Journal on Advances in Signal Processing*, 2020, pp. 1-62, 2020.
- [57] K. Hayashi, Y. Jikumaru, M. Ohsaki, T. Kagaya, Y. Yokosuka, Mean curvature flow for generating discrete surfaces with piecewise constant mean curvatures, *Computer Aided Geometric Design*, 101, p. 102169, 2023.
- [58] M.Z. Alom, T.M. Taha, C. Yakopcic, S. Westberg, P. Sidike, M.S. Nasrin, B.C. Van Esesn, A.A.S. Awwal, V.K. Asari, The history began from alexnet: A comprehensive survey on deep learning approaches, *arXiv preprint arXiv:1803.01164*, 2018.
- [59] R. Anand, T. Shanthi, M. Nithish, S. Lakshman, Face recognition and classification using GoogleNET architecture, *Soft computing for problem solving*, Springer 2020, pp. 261-269.
- [60] X. Xia, C. Xu, B. Nan, Inception-v3 for flower classification, 2017 2nd international conference on image, vision and computing (ICIVC), IEEE, pp. 783-787, 2017.
- [61] G. Huang, Z. Liu, L. Van Der Maaten, K.Q. Weinberger, Densely connected convolutional networks, *Proceedings of the IEEE conference on computer vision and pattern recognition*, pp. 4700-4708, 2017.
- [62] A.G. Howard, M. Zhu, B. Chen, D. Kalenichenko, W. Wang, T. Weyand, M. Andreetto, H. Adam, Mobilenets: Efficient convolutional neural networks for mobile vision applications, *arXiv preprint arXiv:1704.04861*, 2017.
- [63] P. Sun, Y. Lu, J. Zhai, Mapping land cover using a developed U-Net model with weighted cross entropy, *Geocarto International*, 37, pp. 9355-9368, 2022.
- [64] T. Wu, Q. Huang, Z. Liu, Y. Wang, D. Lin, Distribution-balanced loss for multi-label classification in long-tailed datasets, *Computer Vision–ECCV 2020: 16th European Conference, Glasgow, UK, August 23–28, 2020, Proceedings, Part IV 16*, Springer, pp. 162-178, 2020.
- [65] C.H. Sudre, W. Li, T. Vercauteren, S. Ourselin, M. Jorge Cardoso, Generalised dice overlap as a deep learning loss function for highly unbalanced segmentations, *Deep learning in medical image analysis and multimodal learning for clinical decision support*, Springer 2017, pp. 240-248.
- [66] S.S.M. Salehi, D. Erdogmus, A. Gholipour, Tversky loss function for image segmentation using 3D fully convolutional deep networks, *International workshop on machine learning in medical imaging*, Springer, pp. 379-387, 2017.
- [67] S.R. Hashemi, S.S.M. Salehi, D. Erdogmus, S.P. Prabhu, S.K. Warfield, A. Gholipour, Asymmetric loss functions and deep densely-connected networks for highly-imbalanced medical image segmentation: Application to multiple sclerosis lesion detection, *IEEE Access*, 7, pp. 1721-1735, 2018.